

# Extracting electric dipole breakup cross section of one-neutron halo nuclei from inclusive breakup observables

Kazuki Yoshida<sup>1\*</sup>, Tokuro Fukui<sup>1</sup>, Kosho Minomo<sup>2†</sup>, and Kazuyuki Ogata<sup>1</sup>

<sup>1</sup>Research Center for Nuclear Physics, Osaka University, Ibaraki 567-0047, Japan

<sup>2</sup>Department of Physics, Kyushu University, Fukuoka 812-8581, Japan

\*E-mail: yoshidak@rcnp.osaka-u.ac.jp

.....  
 We discuss how to extract an electric dipole (E1) breakup cross section  $\sigma(E1)$  from one-neutron removal cross sections measured at 250 MeV/nucleon by using  $^{12}\text{C}$  and  $^{208}\text{Pb}$  targets,  $\sigma_{-1n}^{\text{C}}$  and  $\sigma_{-1n}^{\text{Pb}}$ , respectively. It is shown that within about 5% error,  $\sigma(E1)$  can be obtained by subtracting  $\Gamma\sigma_{-1n}^{\text{C}}$  from  $\sigma_{-1n}^{\text{Pb}}$ , as assumed in preceding studies. However, for the reaction of weakly-bound projectiles, the scaling factor  $\Gamma$  is found to be about two times as large as that usually adopted. As a result, we obtain 13–20 % smaller  $\sigma(E1)$  of  $^{31}\text{Ne}$  at 250 MeV/nucleon than extracted in a previous analysis of experimental data. By compiling the values of  $\Gamma$  obtained for several projectiles,  $\Gamma = (2.30 \pm 0.41) \exp(-S_n) + (2.43 \pm 0.21)$  is obtained, where  $S_n$  is the neutron separation energy. The target mass number dependence of the nuclear parts of the one-neutron removal cross section and the elastic breakup cross section is also investigated.  
 .....

Subject Index      xxxx, xxx

## 1. Introduction

The neutron halo structure [1, 2], which indicates the breakdown of the saturation property of the nuclear density, is one of the novel properties of unstable nuclei. So far several neutron halo nuclei have been discovered:  $^{11}\text{Be}$ ,  $^{15}\text{C}$ ,  $^{19}\text{C}$ , and  $^{31}\text{Ne}$  are well established one-neutron halo nuclei, and  $^6\text{He}$ ,  $^{11}\text{Li}$ ,  $^{14}\text{Be}$ ,  $^{17}\text{B}$ , and  $^{22}\text{C}$  are known as two-neutron halo nuclei. Nowadays, the neutron halo structure is considered to be a rather *general* feature of unstable nuclei far from the stability line. It is thus important to complete a list of halo nuclei, which is a hot subject in nuclear physics.

One of the most well known probes for the halo structure is the interaction cross section  $\sigma_{\text{I}}$  [1, 2, 3, 4]. In an experiment,  $\sigma_{\text{I}}$  are measured for several isotopes with a target nucleus. A halo nucleus is identified at a mass number where a large increase in  $\sigma_{\text{I}}$  is found. Recently, a fully microscopic analysis of  $\sigma_{\text{I}}$  of Ne isotopes based on the antisymmetrized molecular dynamics (AMD) wave functions [5] and the Melbourne nucleon-nucleon  $g$  matrix [6] was carried out [7]. It was concluded that  $^{31}\text{Ne}$  is a one-neutron halo nucleus with a large deformation of the  $^{30}\text{Ne}$  core. A similar analysis is ongoing for Mg isotopes.

As an alternative probe for the halo structure, it was shown in Ref. [8] that the breakup cross section  $\sigma(E1)$  due to the electric dipole (E1) field can be utilized; it was shown that

<sup>†</sup>Present address: Research Center for Nuclear Physics, Osaka University, Ibaraki 567-0047, Japan

for  $^{19}\text{C}$ , a well-known one-neutron halo nucleus,  $\sigma(\text{E1})$  was indeed large. This is essentially due to the large cross section for the soft dipole excitation that is a characteristic of a halo nucleus. The authors also obtained a large value of  $\sigma(\text{E1})$  for  $^{31}\text{Ne}$ , with which  $^{31}\text{Ne}$  was concluded to be a one-neutron halo nucleus. Since  $\sigma(\text{E1})$  is not an observable, in the analysis the following equation was used to obtain it:

$$\sigma(\text{E1}) = \sigma_{-1n}^{\text{Pb}} - \Gamma\sigma_{-1n}^{\text{C}}, \quad (1)$$

where  $\sigma_{-1n}^{\text{A}}$  is the one-neutron removal cross section by a target nucleus A and  $\Gamma$  is a scaling factor ranging from 1.7 to 2.6 for the  $^{31}\text{Ne}$  projectile. However, no quantitative justification of Eq. (1) for the reaction system was made. Since Eq. (1) is a key formula in the study of Ref. [8], it will be very important to clarify the validity of the equation.

In this paper, we describe one-neutron removal processes by means of sophisticated three-body reaction models: the continuum-discretized coupled-channels method with eikonal approximation (E-CDCC) [9, 10] for the elastic breakup and the eikonal reaction theory (ERT) [11, 12] for the one-neutron stripping. The purpose of the present study is to examine Eq. (1) and find an appropriate value of  $\Gamma$ . There exists a number of works [13, 14, 15, 16, 17, 18, 19, 20, 21, 22, 23, 24] regarding the assumptions behind Eq. (1), i.e., interference between nuclear and Coulomb breakup, role of continuum-continuum couplings, breakup due to the electric quadrupole field, and so forth. Most of them focused on reactions at relatively lower incident energies, where one may expect the above-mentioned ‘‘higher-order’’ effects. In the present study, we consider breakup processes at 250 MeV/nucleon; at such energies, the mechanism of the breakup reaction is believed to be simple. Nevertheless, it will be very important to evaluate possible errors of using Eq. (1) quantitatively. Another important aim of this work is to find a target mass-number ( $A$ ) dependence of  $\sigma_{-1n}$  due to the nuclear interaction, which is essential to determine the scaling factor  $\Gamma$ .

The construction of this paper is as follows. In §2 we briefly recapitulate the formalism of E-CDCC and ERT, and clarify the condition for Eq. (1) to be satisfied. In §3 we examine the assumptions behind Eq. (1) one by one. Then the  $A$ -dependence of  $\sigma_{-1n}$  due to the nuclear interaction is investigated for several projectiles and  $\Gamma$  is evaluated. We present a functional form of  $\Gamma$  with respect to the neutron separation energy  $S_n$ . The  $A$ -dependence of the nuclear part of the elastic breakup cross section is also discussed. Finally, a summary is given in §4.

## 2. Formalism

### 2.1. Three-body system and model space

We describe the one-neutron removal process with a  $c + n + \text{A}$  three-body system shown in Fig. 1;  $c$  and  $n$  are the core nucleus and the valence neutron in the projectile P, respectively, and A is the target nucleus. The coordinates of P,  $c$ , and  $n$  relative to A are denoted by  $\mathbf{R}$ ,  $\mathbf{R}_c$ , and  $\mathbf{R}_n$ , respectively, and  $\mathbf{r}$  represents the coordinate from  $c$  to  $n$ . The three-body Schrödinger equation is given by

$$\left[ -\frac{\hbar^2}{2\mu}\nabla_{\mathbf{R}}^2 + U_n(R_n) + U_c(R_c) + \hat{h} - E \right] \Psi(\mathbf{r}, \mathbf{R}) = 0, \quad (2)$$

where  $\mu$  is the reduced mass of the P-A system,  $U_n$  and  $U_c$  are, respectively, the distorting potentials of  $n$  and  $c$  by A;  $U_c$  consists of the nuclear and Coulomb parts.  $\hat{h}$  is the internal

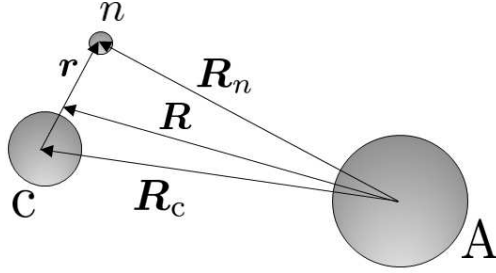


**Fig. 1** Schematic illustration of the  $c + n + A$  three-body system.

Hamiltonian of P and  $E$  is the total energy of the system. We solve Eq. (2) within a model space:

$$\mathfrak{P} \equiv \sum_{i=0}^{i_{\max}} |i\rangle \langle i| \approx 1, \quad (3)$$

where  $|i\rangle$  is the ground state ( $i=0$ ) or a discretized continuum state ( $i>0$ ) of P. Equation (3) means that approximately  $\mathfrak{P}$  can be regarded as a complete set for describing a reaction process considered in the present study [25].

### 2.2. Continuum-discretized coupled-channels method with eikonal approximation (E-CDCC)

In E-CDCC [9, 10], the total wave function  $\Psi(\mathbf{r}, \mathbf{R})$  is described by

$$\Psi(\mathbf{r}, \mathbf{R}) = \sum_i \frac{1}{\sqrt{\hbar v_i}} e^{i(K_i z + \eta_i \ln(K_i R - K_i z))} \psi_i(b, z) \phi_i(\mathbf{r}), \quad (4)$$

where  $\phi_i(\mathbf{r})$  is the wave function of P in the  $i$ th state satisfying  $\hat{h}\phi_i(\mathbf{r}) = \varepsilon_i \phi_i(\mathbf{r})$ ,  $K_i$  ( $v_i$ ) is the relative wave number (velocity) between P and A, and  $\eta_i$  is the Sommerfeld parameter.  $b$  is the impact parameter and  $\phi_R$  is the azimuthal angle of  $\mathbf{R}$ . The  $z$ -axis is taken to be the incident direction. For simplicity, in Eq. (4) the  $\phi_R$  dependence of the wave function is dropped. It should be noted that the monopole Coulomb interaction between P and A is taken into account by using the Coulomb incident wave function in Eq. (4).

After solving the E-CDCC equation, Eq. (4.5) of Ref. [25], with the boundary condition  $\lim_{z \rightarrow -\infty} \psi_i(b, z) = \sqrt{\hbar v_0} \delta_{i0}$ , one obtains the eikonal  $S$ -matrix element

$$S_i(b) = \frac{1}{\sqrt{\hbar v_0}} \lim_{z \rightarrow \infty} \psi_i(b, z). \quad (5)$$

The elastic breakup cross section  $\sigma_{\text{EB}}$  is given by

$$\sigma_{\text{EB}} = 2\pi \int \sum_{i \neq 0} |S_i(b)|^2 b db. \quad (6)$$

### 2.3. Eikonal reaction theory (ERT)

ERT [11, 12] is an extended version of CDCC that is applicable to the neutron stripping processes, explicitly taking account of the Coulomb breakup contribution. ERT describes

the total wave function as

$$\Psi(\mathbf{r}, \mathbf{R}) = \frac{1}{\sqrt{\hbar\hat{v}}} e^{i(\hat{K}z + \hat{\eta} \ln(\hat{K}R - \hat{K}z))} \Phi(\mathbf{r}, \mathbf{R}), \quad (7)$$

where the P-A relative wave number is represented by the operator:

$$\hat{K} = \frac{1}{\hbar} \sqrt{2\mu(E - \hat{h})}. \quad (8)$$

Accordingly, the P-A Sommerfeld parameter is treated as an operator. The velocity operator  $\hat{v}$  depends on  $R$  as

$$\hat{v} = \sqrt{\frac{2}{\mu} \left( E - \hat{h} - \frac{Z_P Z_A e^2}{R} \right)}, \quad (9)$$

which is the operator form of Eq. (4.4) of Ref. [25] multiplied by  $\hbar/\mu$ ;  $Z_P$  ( $Z_A$ ) is the atomic number of P (A). The  $S$  matrix operator in ERT is given by

$$\hat{S} \equiv \exp \left[ \frac{\mathcal{P}}{i} \int_{-\infty}^{\infty} \hat{O}^\dagger(z') [U_n(R_n) + U_c(R_c)] \hat{O}(z') dz' \right], \quad (10)$$

where

$$\hat{O}(z) \equiv \frac{1}{\sqrt{\hbar\hat{v}}} e^{i(\hat{K}z + \hat{\eta} \ln(\hat{K}R - \hat{K}z))} \quad (11)$$

and  $\mathcal{P}$  is the path ordering operator with respect to  $z$ .

Then, the adiabatic approximation  $\hat{h} \rightarrow \varepsilon_0$  is made in Eq. (10) to the term related to  $U_n(R_n)$ , which results in the separation of the  $S$ -matrix operator:

$$\hat{S} \rightarrow \hat{S}_n \hat{S}_c \quad (12)$$

with

$$\hat{S}_n = \exp \left[ \frac{1}{i\hbar v_0} \int_{-\infty}^{\infty} U_n(R_n) dz \right], \quad (13)$$

$$\hat{S}_c = \exp \left[ \frac{\mathcal{P}}{i} \int_{-\infty}^{\infty} \hat{O}^\dagger(z) U_c(R_c) \hat{O}(z) dz \right]. \quad (14)$$

The neutron stripping cross section  $\sigma_{n:\text{STR}}$  is given by

$$\sigma_{n:\text{STR}} = 2\pi \int \langle 0 | |\hat{S}_c|^2 (1 - |\hat{S}_n|^2) | 0 \rangle b db. \quad (15)$$

#### 2.4. Assumptions behind the E1 cross section formula

By definition,  $\sigma_{-1n}$  is the sum of  $\sigma_{\text{EB}}$  and  $\sigma_{n:\text{STR}}$ :

$$\sigma_{-1n} = \sigma_{\text{EB}} + \sigma_{n:\text{STR}}. \quad (16)$$

To extract  $\sigma(\text{E1})$ , first we need the following condition of incoherence between the nuclear and Coulomb breakup:

$$\sigma_{\text{EB}}^{\text{Pb}} \approx \sigma_{\text{EB}(\text{N})}^{\text{Pb}} + \sigma_{\text{EB}(\text{C})}^{\text{Pb}}, \quad (17)$$

where we put (N) and (C) to specify the nuclear and Coulomb parts of  $\sigma_{\text{EB}}$ , respectively. More explicitly,  $\sigma_{\text{EB}(\text{N})}$  ( $\sigma_{\text{EB}(\text{C})}$ ) is the elastic breakup cross section evaluated with dropping the off-diagonal coupling potentials due to the Coulomb (nuclear) interaction in solving

Eq. (2). The second condition is that the coupled-channel effects caused by the Coulomb interaction on the neutron stripping is negligibly small:

$$\sigma_{n:\text{STR}}^{\text{Pb}} \approx \sigma_{n:\text{STR}(\text{N})}^{\text{Pb}}. \quad (18)$$

If Eqs. (17) and (18) are satisfied, we have

$$\sigma_{-1n}^{\text{Pb}} \approx \sigma_{\text{EB}(\text{C})}^{\text{Pb}} + \sigma_{-1n(\text{N})}^{\text{Pb}}, \quad (19)$$

where

$$\sigma_{-1n(\text{N})}^{\text{Pb}} = \sigma_{\text{EB}(\text{N})}^{\text{Pb}} + \sigma_{n:\text{STR}(\text{N})}^{\text{Pb}}. \quad (20)$$

The third condition is given by

$$\sigma_{\text{EB}(\text{C})}^{\text{Pb}} \approx \sigma_{\text{EB}(\text{E1})}^{\text{Pb}} \equiv \sigma(\text{E1}), \quad (21)$$

where EB(E1) means the first-order E1 transition cross section. The fourth and last condition is

$$\sigma_{-1n}^{\text{C}} \approx \sigma_{-1n(\text{N})}^{\text{C}}. \quad (22)$$

One may then obtain Eq. (1) with  $\Gamma$  defined by

$$\Gamma = \frac{\sigma_{-1n(\text{N})}^{\text{Pb}}}{\sigma_{-1n(\text{N})}^{\text{C}}}. \quad (23)$$

### 3. Results and discussion

#### 3.1. Model setting

We consider neutron removal processes of projectiles having a  $n$ - $c$  structure by  $^{12}\text{C}$ ,  $^{16}\text{O}$ ,  $^{48}\text{Ca}$ ,  $^{58}\text{Ni}$ ,  $^{90}\text{Zr}$ , and  $^{208}\text{Pb}$  at 250 MeV/nucleon. We take a central Woods-Saxon (WS) potential between the  $n$ - $c$  pair. The radius parameter  $r_0$  and the diffuseness parameter  $a_0$  together with the  $n$ - $c$  relative angular momentum  $\ell$  in the ground state,  $\ell_0$ , and  $S_n$  are shown in Table 1. The depth of the WS potential is determined to reproduce  $S_n$ . The maximum value  $\ell_{\text{max}}$  of  $\ell$  is set to 3. For each  $\ell$ , the continuum state up to  $k = 0.66 \text{ fm}^{-1}$ , where  $k$  is the  $n$ - $c$  relative wave number, is discretized by the momentum-bin method with an equal increment  $\Delta k$ . We take  $\Delta k = 0.066 \text{ fm}^{-1}$  for  $\ell \neq 0$  and  $\Delta k = 0.033 \text{ fm}^{-1}$  for  $\ell = 0$ . The maximum value of  $r$  is set to 200 fm.

The distorting potential  $U_n$  ( $U_c$ ) is evaluated by a microscopic single (double) folding model; the Melbourne nucleon-nucleon  $g$  matrix [6] and the Hartree-Fock (HF) wave functions of  $c$  and  $A$  based on the Gogny D1S force [29, 30] are adopted. This microscopic approach has successfully been applied to several reaction systems [7, 25, 31]. The maximum impact parameter  $b_{\text{max}}$  is taken to be 50 fm for nuclear breakup processes, whereas we put  $b_{\text{max}} = 400 \text{ fm}$  when Coulomb breakup is included.

**Table 1** Inputs for the  $n$ - $c$  pair.

	$r_0$ [fm]	$a_0$ [fm]	$\ell_0$	$S_n$ [MeV]	Ref.
$^{11}\text{Be}$	1.39	0.52	0	0.503	[21]
$^{15}\text{C}$	1.10	0.60	0	1.218	[26]
$^{19}\text{C}$	1.25	0.70	0	0.580	[27]
$^{31}\text{Ne}$	1.25	0.75	1	0.330	[28]

**Table 2** Cross sections for each projectile (in the unit of mb).

P	$\sigma_{\text{EB}}^{\text{Pb}}$	$\sigma_{\text{EB(N)}}^{\text{Pb}}$	$\sigma_{\text{EB(C)}}^{\text{Pb}}$	$\sigma_{\text{EB(E1)}}^{\text{Pb}}$	$\sigma_{n:\text{STR}}^{\text{Pb}}$	$\sigma_{n:\text{STR(N)}}^{\text{Pb}}$	$\sigma_{-1n}^{\text{C}}$	$\sigma_{-1n(\text{N})}^{\text{C}}$
$^{11}\text{Be}$	754	108	670	680	364	347	113	110
$^{15}\text{C}$	445	39	418	423	213	196	77	72
$^{19}\text{C}$	769	81	694	701	308	321	99	94
$^{31}\text{Ne}$	812	61	752	758	268	256	87	82

**Table 3** Errors of the conditions of Eqs. (17), (18), (21), and (22) are shown as  $f_1$ ,  $f_2$ ,  $f_3$ , and  $f_4$ , respectively.  $\sigma(\text{E1})$  evaluated by Eqs. (23) and (1) is also shown in the unit of mb.  $f_{\text{tot}}$  is the total error of Eq. (1). See the text for detail.

P	$f_1$	$f_2$	$f_3$	$f_4$	$\sigma(\text{E1})$	$f_{\text{tot}}$
$^{11}\text{Be}$	3.2%	4.6%	1.5%	2.4%	663	4.1%
$^{15}\text{C}$	2.6%	7.9%	1.2%	6.5%	423	3.8%
$^{19}\text{C}$	0.8%	4.2%	1.0%	5.1%	676	6.7%
$^{31}\text{Ne}$	0.1%	4.5%	0.8%	5.9%	763	1.9%

### 3.2. Examination of the E1 cross section formula

We show in Table 2 several cross sections discussed in Sec. 2.4 for the  $^{11}\text{Be}$ ,  $^{15}\text{C}$ ,  $^{19}\text{C}$ , and  $^{31}\text{Ne}$  projectiles and the  $^{12}\text{C}$  and  $^{208}\text{Pb}$  targets evaluated by E-CDCC and ERT. In Table 3  $f_1$ ,  $f_2$ ,  $f_3$ , and  $f_4$ , the errors of the conditions of Eqs. (17), (18), (21), and (22), respectively, are shown;  $f_i$  ( $i = 1-4$ ) is the relative difference between the results on the left-hand-side and the right-hand-side on each equation. The value of  $\sigma(\text{E1})$  corresponding to Eqs. (1) and (23) is evaluated by subtracting  $\sigma_{-1n(\text{N})}^{\text{Pb}}$  from  $\sigma_{-1n}^{\text{Pb}}$ . By taking the relative difference between  $\sigma(\text{E1})$  thus obtained and  $\sigma_{\text{EB(E1)}}^{\text{Pb}}$  calculated by E-CDCC, we get the total error  $f_{\text{tot}}$  of Eq. (1). One sees all of the errors are below 8% for the breakup of these one-neutron halo nuclei at 250 MeV/nucleon, which validates the use of Eq. (1) for the systems. On average,  $f_1$  and  $f_3$  are less than a few percent, whereas  $f_2$ ,  $f_4$ , and  $f_{\text{tot}}$  are about 5%.

The small  $f_1$ , i.e., small nuclear and Coulomb interference, can be understood as follows. First, because of the dominance of the E1 coupling, the  $\ell$  value after the Coulomb breakup is concentrated to  $|\ell_0 \pm 1|$ . In fact, more than 97% of  $\sigma_{\text{EB(C)}}^{\text{Pb}}$  for  $^{11}\text{Be}$  ( $\ell_0 = 0$ ) by  $^{208}\text{Pb}$  comes from the  $p$ -wave breakup cross section. On the other hand, there is no such selection for the nuclear breakup; about 3/4 of  $\sigma_{\text{EB(N)}}^{\text{Pb}}$  goes to  $\ell \neq 1$ . Second, as an important aspect of the present study, we discuss the cross section integrated over the scattering angle. Then there is no interference between different values of  $b$ . It is well known that nuclear breakup amplitude is concentrated at the nuclear surface, whereas the E1 amplitude has a very long tail with respect to  $b$ . Therefore, the nuclear and Coulomb breakup processes occur at different  $b$  and populate different  $\ell$  of the breakup state, which results in small nuclear-Coulomb interference. It should be noted that if an angular distribution of the breakup cross section is discussed, because of the coherence of the breakup amplitudes at different  $b$ , one can expect non-negligible nuclear-Coulomb interference even at 250 MeV/nucleon.

**Table 4** Cross sections for the  ${}^8\text{B}$  breakup by  ${}^{208}\text{Pb}$  (in the unit of mb).

$\sigma_{\text{EB}}^{\text{Pb}}$	$\sigma_{\text{EB(N)}}^{\text{Pb}}$	$\sigma_{\text{EB(C)}}^{\text{Pb}}$	$\sigma_{\text{EB(E1)}}^{\text{Pb}}$	$\sigma_{\text{EB(E2)}}^{\text{Pb}}$
254	27	258	228	46

Equation (18) is expected to hold because, as mentioned above,  $\sigma_{n\text{-STR}}$  is due to  $U_n(R_n)$  unless strong coupled-channel effects caused by the Coulomb interaction exist. The small  $f_2$  obtained will support this picture. For  $f_3$ , an important point of the present analysis is that we consider one-neutron halo nuclei, for which the E2 effective charge  $e_{\text{E2}}$  is much smaller than the E1 effective charge  $e_{\text{E1}}$ . Because the E1 coupling strength is small and the scattering energy is relatively high, one may expect that Eq. (21) holds well, which is indeed the case as shown in Table 3. It should be noted that the very large E1 breakup cross section by  ${}^{208}\text{Pb}$  is due to the long-range nature of its amplitude, not to its strength. Note also that in the present study deformation effects of  $c$  are neglected; the coupling between the  $0^+$  and  $2^+$  states of  $c$  can change the E2 transition amplitude. Inclusion of the core deformation in E-CDCC and ERT following the recent works [32, 33] will be interesting and important future work.

The conclusions summarized in Table 3 change if we consider a proton “halo” nucleus, e.g.,  ${}^8\text{B}$ . In Table 4 several cross sections for the  ${}^8\text{B}$  breakup by  ${}^{208}\text{Pb}$  at 250 MeV/nucleon are shown;  $r_0 = 1.25$  fm,  $a_0 = 0.52$  fm,  $\ell_0 = 1$ , and the proton separation energy of 0.137 MeV are used [21]. One sees the E2 contribution  $\sigma(\text{E2})$  is about 20% of  $\sigma(\text{E1})$ . This is essentially because  $e_{\text{E2}}$  of  ${}^8\text{B}$  is about 2.7 times as large as its  $e_{\text{E1}}$ . Then, the higher-order effect reduces the sum of  $\sigma(\text{E1})$  and  $\sigma(\text{E2})$  by about 5%. This somewhat large higher-order effect is due to the large E2 coupling strength compared with the E1 strength. In fact, if we perform an all-order calculation including just the E1 coupling, we obtain 220 mb that is smaller than  $\sigma(\text{E1})$  by only 3%. We have thus the addition of  $\sigma(\text{E2})$  to  $\sigma(\text{E1})$  and the decrease in the first-order Coulomb breakup cross section,  $\sigma(\text{E1}) + \sigma(\text{E2})$ , due to higher-order processes. In the end,  $\sigma(\text{E1})$  is smaller than  $\sigma_{\text{EB(C)}}^{\text{Pb}}$  by about 13% even at 250 MeV/nucleon. The nuclear-Coulomb interference of about 12% also appears for  ${}^8\text{B}$  because of the less selectivity of  $\ell$ . Therefore, we conclude that we have less validity of Eq. (1) for  $c + p$  nuclei, even if we consider inclusive breakup observables measured at 250 MeV/nucleon.

### 3.3. Target mass number dependence of one-neutron removal cross section due to nuclear interaction

It is shown in Sec. 3.2 that at 250 MeV/nucleon Eq. (1) holds well for one-neutron halo nuclei with  $\Gamma$  given by Eq. (23). Before evaluating  $\Gamma$ , we see the  $A$ -dependence of  $\sigma_{-1n(N)}^A$ . We here consider not only the four well-established one-neutron halo nuclei listed in Table 2 but also

**Table 5** Parameters for the  $n$ - $c$  pairs.

	${}^{29}\text{Ne}$	${}^{33}\text{Mg}$	${}^{35}\text{Mg}$	${}^{37}\text{Mg}$	${}^{39}\text{Si}$	${}^{41}\text{Si}$
$\ell_0$	0	1	1	0 or 1	1	1
$S_n$ [MeV]	1.260	2.640	1.011	0.489	2.080	0.300

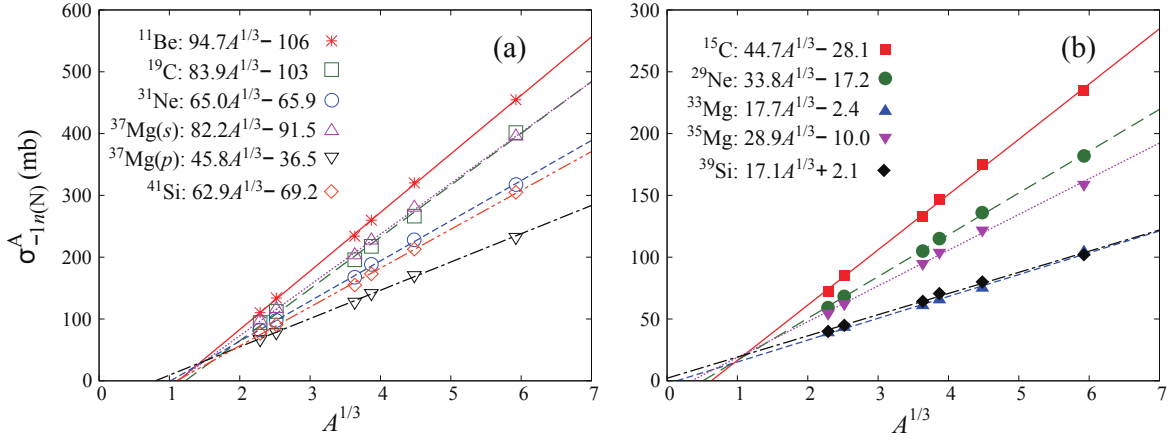


**Fig. 2**  $\sigma_{-1n(N)}^A$  as a function of  $A^{1/3}$ . Panels (a) and (b) correspond to the projectiles having  $S_n < 1.0$  MeV and  $S_n > 1.0$  MeV, respectively.

$^{29}\text{Ne}$ ,  $^{33}\text{Mg}$ ,  $^{35}\text{Mg}$ ,  $^{37}\text{Mg}$ ,  $^{39}\text{Si}$ , and  $^{41}\text{Si}$ . The newly added six projectiles are expected to have a  $c + n$  structure with a (moderately) small value of  $S_n$ ; the input parameters for them are shown in Table 5. We take  $r_0 = 1.20$  fm and  $a_0 = 0.70$  fm for all the systems. For  $^{37}\text{Mg}$  we assume two possibilities of  $\ell_0$ , i.e.,  $^{37}\text{Mg}(s)$  ( $s$ -wave) and  $^{37}\text{Mg}(p)$  ( $p$ -wave). The values of  $S_n$  for the Mg isotopes are taken from Ref. [34] and those for the other nuclei are from Ref. [35]; for  $^{41}\text{Si}$  that has a negative mean value of  $S_n$  [35] we use  $S_n = 0.3$  MeV.

We show in Fig. 2  $\sigma_{-1n(N)}^A$  as a function of  $A^{1/3}$ . Panels (a) and (b) correspond to the projectiles having  $S_n$  smaller and larger than 1 MeV, respectively. Clearly  $\sigma_{-1n(N)}^A$  follows the scaling law of  $A^{1/3}$  for all the projectiles. In each panel the result of a fitting by  $a_P A^{1/3} + b_P$  is given. It should be noted that  $a_P$  and  $b_P$  have a rather strong dependence on  $P$ .

The success of the  $a_P A^{1/3} + b_P$  scaling of  $\sigma_{-1n(N)}^A$  suggests

$$\Gamma = \frac{\bar{a}_P R_{Pb} + b_P}{\bar{a}_P R_C + b_P} = \frac{R_{Pb} + \bar{b}_P}{R_C + \bar{b}_P}, \quad (24)$$

where  $R_A$  is the radius of the nucleus  $A$ ,  $\bar{a}_P \sim 1.2a_P$ , and  $\bar{b}_P \equiv b_P/\bar{a}_P$ . Apparently  $\bar{b}_P$  is related to an effective radius of  $P$ , which naively suggests  $0 \leq \bar{b}_P \leq R_P$ . In fact,  $\Gamma$  is considered in Ref. [8] to be in the range of

$$\frac{R_{Pb} + R_P}{R_C + R_P} \leq \Gamma \leq \frac{R_{Pb}}{R_C}. \quad (25)$$

The lower limit corresponds to the strong absorption limit and the upper limit to the picture of the Serber model [36]. Our present calculation suggests, however, that  $\bar{b}_P$  can be negative, which results in  $\Gamma$  larger than the upper limit of Eq. (25).

The results of  $\Gamma$  are shown in Table 6 and plotted in Fig. 3 as a function of  $S_n$ ; in the figure the range of  $\Gamma$  assumed in Ref. [8], Eq. (25), is shown by a bar for each  $P$ . One sees that  $\Gamma$  is

**Table 6** The scaling factor  $\Gamma$  for the projectiles.

	$^{11}\text{Be}$	$^{15}\text{C}$	$^{19}\text{C}$	$^{29}\text{Ne}$	$^{31}\text{Ne}$	$^{33}\text{Mg}$	$^{35}\text{Mg}$	$^{37}\text{Mg}(s)$	$^{37}\text{Mg}(p)$	$^{39}\text{Si}$	$^{41}\text{Si}$
$\Gamma$	4.12	3.26	4.26	3.07	3.86	2.68	2.91	4.05	3.45	2.56	3.98



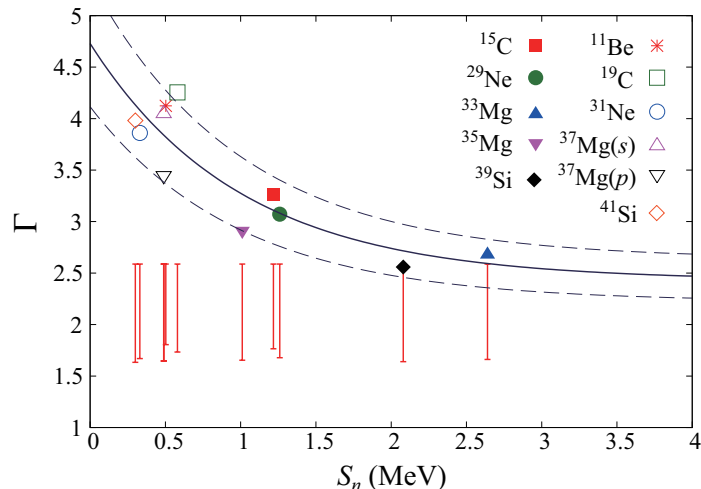


**Fig. 3** Plot of  $\Gamma$  as a function of  $S_n$ . The vertical bars show the range of  $\Gamma$  given by Eq. (25). The result of a functional fit of Eq. (26) is also shown.

located around 4 when  $S_n < 1$  MeV and decreases as  $S_n$  increases, toward the upper limit of Eq. (25). It is found that  $\Gamma$  is well fitted by

$$\Gamma = (2.30 \pm 0.41)e^{-S_n} + (2.43 \pm 0.21), \quad (26)$$

which is shown by the solid and dashed curves in Fig. 3. This simple functional form can be helpful for practical use.

As shown in Fig. 3, for  $^{31}\text{Ne}$  (open circle) the result of  $\Gamma$  of the present study is almost two times as large as the mean value adopted in the previous study [8]. Consequently, we obtain about 13% (20%) smaller  $\sigma(\text{E1})$  than that evaluated with the maximum (minimum) value of  $\Gamma$ , 2.6 (1.7), of Eq. (25). It should be noted that in the present study we do not consider a spectroscopic factor  $\mathcal{S}$ ; we assume  $\mathcal{S} = 1$  for all the projectiles. One may obtain  $\mathcal{S}$  by comparing the theoretical cross section with experimental data, as in Refs. [11, 28]. In this study, however, we focus on the  $A$ -dependence of the cross sections and the values of  $\Gamma$ . It is rather obvious that  $\mathcal{S}$  has very small effect on them. To be accurate, the one-neutron removal process for a projectile having a loosely-bound neutron is peripheral. Thus, what is to be determined through the reaction analysis is not  $\mathcal{S}$  but the asymptotic normalization coefficient (ANC). As shown in Fig. 1 of Ref. [11], the ANC evaluated by the experimental data [8] has very weak  $A$ -dependence. Therefore, even though a rather naive structural model of the projectiles is adopted in this study, the conclusions drawn above are expected to be quite robust.

### 3.4. Scaling of nuclear elastic breakup cross section

In this subsection we discuss the  $A$ -dependence of  $\sigma_{\text{EB}(N)}$ , considering a possibility of extracting  $\sigma(\text{E1})$  from *exclusive* breakup observables [37, 38, 39]. Though it is widely believed that  $\sigma_{\text{EB}(N)}$  follows the  $A^{1/3}$  scaling [21], there exist several works that report different results [16, 22, 12]. In this paper we follow the prescription of Ref. [12]. First, we determine the effective radius  $R_{\text{EB}}$  from the peak of the integrand of Eq. (6) divided by  $b$ . Then the

effective width  $D_{\text{EB}}$  is evaluated by  $D_{\text{EB}} = \sigma_{\text{EB(N)}}/(2\pi R_{\text{EB}})$ . By looking at the  $A$ -dependence of  $R_{\text{EB}}$  and  $D_{\text{EB}}$ , one can see the  $A$ -dependence of  $\sigma_{\text{EB(N)}}$ .

It is found, as in Ref. [12], that both  $R_{\text{EB}}$  and  $D_{\text{EB}}$  are fitted well by the  $\alpha_X A^{1/3} + \beta_X$  form ( $X$  is  $R$  or  $D$ ). The values of  $\alpha_R$ ,  $\beta_R$ ,  $\alpha_D$ ,  $\beta_D$  are given in Table 7. The resulting functional form of  $\sigma_{\text{EB(N)}}$  is

$$\sigma_{\text{EB(N)}} = 2\pi(\alpha_R A^{1/3} + \beta_R)(\alpha_D A^{1/3} + \beta_D) \equiv c_2 A^{2/3} + c_1 A^{1/3} + c_0. \quad (27)$$

In Fig. 4 we compare Eq. (27) with  $\sigma_{\text{EB(N)}}$  obtained by E-CDCC for the six target nuclei, as in Fig. 2. One sees clearly that Eq. (27) works well for all the projectiles. In the sixth column of Table 7, we show  $c_2/c_1$  that gives a deviation from the  $A^{1/3}$  scaling formula. In all the cases  $c_2/c_1$  is larger than several tens of percent. For  $^{11}\text{Be}$  and  $^{19}\text{C}$  we have  $|c_2/c_1| \sim 4$ , which indicates the dominance of the  $A^{2/3}$  dependence.

One of the key ingredients for the  $A$ -dependence of  $\sigma_{\text{EB(N)}}$  is the c-A distorting potential, which is microscopically calculated in the present study. Note that the microscopic double folding model used has successfully been applied to several reaction processes at around 250 MeV/nucleon [25, 31]. If we adopt the parameters for the  $^{10}\text{Be}$ -A system given in Table I of Ref. [21], we obtain a similar result to that of Ref. [21], i.e., the  $A^{1/3}$  scaling. Another important aspect of the present study is the incident energy, i.e., 250 MeV/nucleon. If we evaluate  $\sigma_{\text{EB(N)}}$  of  $^{11}\text{Be}$  at 70 MeV/nucleon by E-CDCC with microscopic distorting potentials calculated at the energy, we have an  $A$ -dependence slightly weaker than  $A^{1/3}$ ; this is consistent with the result of Ref. [22]. Further investigation will be necessary to draw a definite conclusion on the  $A$ -dependence of  $\sigma_{\text{EB(N)}}$ . At this stage, it is difficult to find a simple formula to extract  $\sigma(\text{E1})$  from exclusive breakup observables, i.e.,  $\sigma_{\text{EB}}^{\text{Pb}}$  and  $\sigma_{\text{EB}}^{\text{C}}$ .

Additionally, we remark the importance of Coulomb breakup by a  $^{12}\text{C}$  target. We show  $\sigma_{\text{EB}}^{\text{C}}$ ,  $\sigma_{\text{EB(N)}}^{\text{C}}$ , and the ratio  $\sigma_{\text{EB(N)}}^{\text{C}}/\sigma_{\text{EB}}^{\text{C}}$  in Table 7. One sees that  $\sigma_{\text{EB(N)}}^{\text{C}}/\sigma_{\text{EB}}^{\text{C}}$  is considerably smaller than unity. Thus, we need to consider the contribution from Coulomb breakup of

**Table 7** Fitting parameters of the effective radius and width of  $\sigma_{\text{EB(N)}}$  given in the unit of fm.  $c_2/c_1$  shows the importance of the  $A^{2/3}$  dependence compared to the  $A^{1/3}$  dependence.  $\sigma_{\text{EB}}^{\text{C}}$  and  $\sigma_{\text{EB(N)}}^{\text{C}}$  (in the unit of mb) and its ratio  $\sigma_{\text{EB(N)}}^{\text{C}}/\sigma_{\text{EB}}^{\text{C}}$  are also shown. See the text for details.

	$\alpha_R$	$\beta_R$	$\alpha_D \times 100$	$\beta_D \times 100$	$c_2/c_1$	$\sigma_{\text{EB}}^{\text{C}}$	$\sigma_{\text{EB(N)}}^{\text{C}}$	$\sigma_{\text{EB(N)}}^{\text{C}}/\sigma_{\text{EB}}^{\text{C}}$
$^{11}\text{Be}$	1.79	1.13	3.03	-2.76	-3.58	15.13	12.67	0.837
$^{15}\text{C}$	1.41	3.33	1.16	-1.43	0.886	7.41	4.59	0.620
$^{19}\text{C}$	1.70	2.54	2.26	-2.81	3.99	12.01	8.77	0.731
$^{29}\text{Ne}$	1.29	4.50	0.980	-1.39	0.483	6.27	3.78	0.599
$^{31}\text{Ne}$	1.61	3.91	1.67	-2.65	1.19	9.32	5.58	0.603
$^{33}\text{Mg}$	1.39	4.20	0.270	-0.240	0.469	2.75	1.44	0.525
$^{35}\text{Mg}$	1.37	4.75	0.700	-0.990	0.487	5.11	2.77	0.542
$^{37}\text{Mg}(s)$	1.37	4.73	2.70	-4.59	0.571	13.15	8.21	0.624
$^{37}\text{Mg}(p)$	1.28	5.21	1.30	-2.20	0.421	7.16	4.03	0.563
$^{39}\text{Si}$	1.23	5.00	0.360	-0.430	0.348	3.32	1.71	0.514
$^{41}\text{Si}$	1.31	5.20	1.83	-3.34	0.466	9.48	5.03	0.530

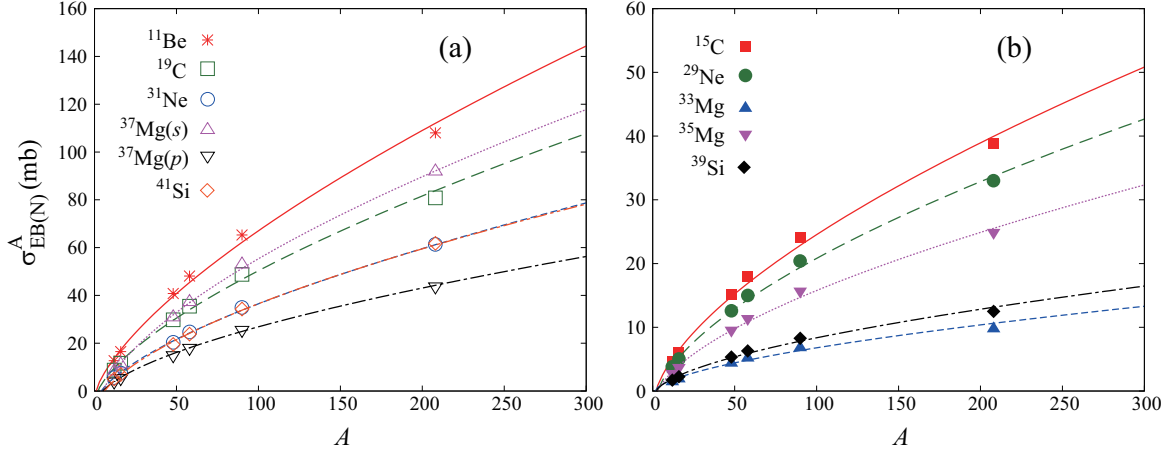


**Fig. 4** Same as in Fig. 2 but for  $\sigma_{\text{EB(N)}}^A$  and plotted as a function of  $A$ .

several tens of percent, when we consider elastic breakup processes of a projectile consisting of a core nucleus and a loosely-bound neutron by  $^{12}\text{C}$  at 250 MeV/nucleon.

#### 4. Summary

We have examined the E1 cross section formula, Eq. (1), by describing the one-neutron removal process at 250 MeV/nucleon with three-body reaction models. The elastic breakup and the one-neutron stripping are described by the continuum-discretized coupled-channels method with the eikonal approximation (E-CDCC) and the eikonal reaction theory (ERT), respectively. We took  $^{11}\text{Be}$ ,  $^{15}\text{C}$ ,  $^{19}\text{C}$ ,  $^{29}\text{Ne}$ ,  $^{31}\text{Ne}$ ,  $^{33}\text{Mg}$ ,  $^{35}\text{Mg}$ ,  $^{37}\text{Mg}$ ,  $^{39}\text{Si}$ , and  $^{41}\text{Si}$  for the projectile, and  $^{12}\text{C}$ ,  $^{16}\text{O}$ ,  $^{48}\text{Ca}$ ,  $^{58}\text{Ni}$ ,  $^{90}\text{Zr}$ , and  $^{208}\text{Pb}$  for the target nucleus.

Four conditions behind Eq. (1) are clarified and validated one by one within about 5% error for the breakup of one-neutron halo projectiles at 250 MeV/nucleon. The scaling factor  $\Gamma$  is defined by the ratio of the one-neutron removal cross section for the  $^{208}\text{Pb}$  target due to nuclear interactions,  $\sigma_{-1n(\text{N})}^{\text{Pb}}$ , to that for the  $^{12}\text{C}$  target,  $\sigma_{-1n(\text{N})}^{\text{C}}$ . It is found that  $\sigma_{-1n(\text{N})}$  follows the  $aA^{1/3} + b$  form, where  $A$  is the target mass number, as assumed in preceding studies. The constant  $b$  of the formula, however, is shown to be negative for almost all the projectiles considered. This gives somewhat large enhancement of  $\Gamma$ . We obtained  $\Gamma$  for  $^{31}\text{Ne}$  that is about two times as large as the mean value used in the previous analysis. Consequently, the E1 cross section of  $^{31}\text{Ne}$  is reduced by 13–20 %. We have found the following functional form of  $\Gamma$ :  $\Gamma = (2.30 \pm 0.41) \exp(-S_n) + (2.43 \pm 0.21)$  with  $S_n$  the neutron separation energy.

The  $A$ -dependence of the nuclear elastic-breakup cross section  $\sigma_{\text{EB(N)}}^A$  is also investigated. It is found that  $\sigma_{\text{EB(N)}}^A$  follows  $c_2 A^{2/3} + c_1 A^{1/3} + c_0$ , i.e., mixture of the  $A^{2/3}$  and  $A^{1/3}$  scaling. Furthermore, contribution of the Coulomb breakup of several tens of percent, which is often neglected, is clarified in the breakup of projectiles having a loosely-bound neutron by the  $^{12}\text{C}$  target. At this stage, it is quite difficult to find a simple formula to extract the E1 cross section from exclusive elastic breakup observables.

---

## Acknowledgment

The authors thank M. Yahiro for valuable comments on this study, and M. Kimura and S. Watanabe for providing information on Mg isotopes. This research was supported in part by Grant-in-Aid of the Japan Society for the Promotion of Science (JSPS).

## References

- [1] I. Tanihata, H. Hamagaki, O. Hashimoto, Y. Shida, N. Yoshikawa, K. Sugimoto, O. Yamakawa, T. Kobayashi, and N. Takahashi, *Phys. Rev. Lett.* **55**, 2676 (1985).
- [2] I. Tanihata, H. Savajols, and R. Kanungo, *Prog. Part. Nucl. Phys.* **68**, 215 (2013).
- [3] K. Tanaka et al., *Phys. Rev. Lett.* **104**, 062701 (2010).
- [4] M. Takechi et al., *Phys. Lett.* **B707**, 357 (2012).
- [5] Y. Kanada-En'yo, M. Kimura, and A. Ono, *Prog. Theor. Exp. Phys.* **2012**, 01A202 (2012), and references therein.
- [6] K. Amos, P. J. Dortmans, H. V. von Geramb, S. Karataglidis, and J. Raynal, *Adv. Nucl. Phys.* **25**, 275 (2000).
- [7] K. Minomo, T. Sumi, M. Kimura, K. Ogata, Y. R. Shimizu, and M. Yahiro, *Phys. Rev. Lett.* **108**, 052503 (2012).
- [8] T. Nakamura *et al.*, *Phys. Rev. Lett.* **103**, 262501 (2009).
- [9] K. Ogata, M. Yahiro, Y. Iseri, T. Matsumoto, and M. Kamimura, *Phys. Rev. C* **68**, 064609 (2003).
- [10] K. Ogata, S. Hashimoto, Y. Iseri, M. Kamimura, and M. Yahiro, *Phys. Rev. C* **73**, 024605 (2006).
- [11] M. Yahiro, K. Ogata, and K. Minomo, *Prog. Theor. Phys.* **126**, 167 (2011).
- [12] S. Hashimoto, M. Yahiro, K. Ogata, K. Minomo, and S. Chiba, *Phys. Rev. C* **83**, 054617 (2011).
- [13] R. Shyam and I. J. Thompson, *Phys. Rev. C* **59**, 2645 (1999).
- [14] F. M. Nunes and I. J. Thompson, *Phys. Rev. C* **59**, 2652 (1999).
- [15] H. Esbensen and G. F. Bertsch, *Phys. Rev. C* **59**, 3240 (1999).
- [16] M. A. Nagarajan, C. H. Dasso, S. M. Lenzi, and A. Vitturi, *Phys. Lett.* **B503**, 65 (2001).
- [17] A. Volya and H. Esbensen, *Phys. Rev. C* **66**, 044604 (2002).
- [18] H. Esbensen and G. F. Bertsch, *Phys. Rev. C* **66**, 044609 (2002).
- [19] R. Chatterjee and R. Shyam, *Phys. Rev. C* **66**, 061601(R) (2002).
- [20] J. Margueron, A. Bonaccorso, and D. M. Brink, *Nucl. Phys.* **A703**, 105 (2002).
- [21] M. S. Hussein, R. Lichtenthaler, F. M. Nunes, and I. J. Thompson, *Phys. Lett.* **B640**, 91 (2006).
- [22] K. Ogata, T. Matsumoto, Y. Iseri, and M. Yahiro, *J. Phys. Soc. Jpn.* **78**, 084201 (2009).
- [23] Y. Kucuk and A. M. Moro, *Phys. Rev. C* **86**, 034601 (2012).
- [24] R. Kumar and A. Bonaccorso, *Phys. Rev. C* **86**, 061601(R) (2012).
- [25] M. Yahiro, K. Ogata, T. Matsumoto, and K. Minomo, *Prog. Theor. Exp. Phys.* **2012**, 01A206 (2012), and references therein.
- [26] P. Capel, H. Esbensen, and F. M. Nunes, *Phys. Rev. C* **85**, 044604 (2012).
- [27] Y. Kondo et al., *Phys. Rev. C* **79**, 014602 (2009).
- [28] W. Horiuchi, Y. Suzuki, P. Capel, and D. Baye, *Phys. Rev. C* **81**, 024606 (2010).
- [29] J. Decharge and D. Gogny, *Phys. Rev. C* **21**, 1568 (1980).
- [30] J. F. Berger, M. Girod, and D. Gogny, *Comp. Phys. Comm.* **63**, 1365 (1991).
- [31] T. Sumi, K. Minomo, S. Tagami, M. Kimura, T. Matsumoto, K. Ogata, Y. R. Shimizu, and M. Yahiro, *Phys. Rev. C* **85**, 064613 (2012).
- [32] A. M. Moro and J. A. Lay, *Phys. Rev. Lett.* **109**, 232502 (2012).
- [33] J. A. Lay, A. M. Moro, J. M. Arias, and Y. Kanada-En'yo, *Phys. Rev. C* **89**, 014333 (2014).
- [34] S. Watanabe *et al.*, *Phys. Rev. C* (to be published), arXiv:1404.2373 (2012).
- [35] G. Audi, A. H. Wapstra, and C. Thibault, *Nucl. Phys.* **A729**, 337 (2003).
- [36] R. Serber, *Phys. Rev.* **72**, 1008 (1947).
- [37] N. Fukuda *et al.*, *Phys. Rev. C* **70**, 054606 (2004).
- [38] T. Aumann *et al.*, *Phys. Rev. C* **59**, 1252 (1999).
- [39] R. Palit *et al.*, *Phys. Rev. C* **68**, 034318 (2003).